

Flux Conversion and Evidence of Relaxation in a High- β Plasma Formed by High-Speed Injection into a Mirror Confinement Structure

H. Y. Guo, A. L. Hoffman, K. E. Miller, and L. C. Steinhauer

Redmond Plasma Physics Laboratory, University of Washington, Seattle, Washington 98195, USA

(Received 21 March 2003; revised manuscript received 14 August 2003; published 16 June 2004)

High- β plasmoids can survive the violent dynamics of supersonic reflection off mirror structures, producing a stable high- β field-reversed configuration (FRC). This shows both the robustness of FRCs and their tendency to assume a preferred plasma state, possibly conforming to a relaxation principle. The key observations are (1) approximate preservation of the magnetic helicity, (2) substantial conversion from toroidal to poloidal magnetic flux, (3) substantial toroidal flow, and (4) a high- β quiescent final state. These results are from the Translation, Confinement, and Sustainment experiment where a disorganized plasmoid is injected at super-Alfvénic speed into a confinement chamber. After successive reflections from end mirrors, the plasmoid settled into a near-FRC state with high β and low toroidal magnetic field. The flux conversion and helicity preservation are inferred by an interpretive model.

DOI: 10.1103/PhysRevLett.92.245001

PACS numbers: 52.55.Lf, 52.30.Ex, 52.55.Dy

Experimental “relaxed” plasma states were first identified 30 years ago [1]. Taylor conjectured that a plasma may relax to a state of minimum magnetic energy $W_m = \int d\tau B^2/2\mu_0$ subject to fixed magnetic helicity, $K_m = \int d\tau \mathbf{A} \cdot \nabla \times \mathbf{A}$: \mathbf{A} is the vector potential, $\mathbf{B} = \nabla \times \mathbf{A}$ is the magnetic field; the integrals are on the system volume. Experiments confirmed the approximate preservation of K_m , and the appearance of relaxed states with current density $\mathbf{j} = \text{const} \times \mathbf{B}$ in agreement with the Taylor principle. These states arise spontaneously in reversed field pinches and in spheromaks, but have $\beta = 0$ (zero pressure). However, since most plasmas have finite β , several more general relaxation principles have been advanced. These include the *modern* relaxation principle [2,3] and the *coercive-functional* principle [4] (both based on a two-fluid plasma model) as well as others. Although various relaxation principles have been proposed, none has been verified by experiment, largely because of the limited diagnostics available in high- β experiments. Hints of field-reversed configuration (FRC) relaxation appeared in the TS-3 device [5] at the University of Tokyo and the Swarthmore Spheromak Experiment [6], which used the counterhelicity spheromak merging formation method. Either a spheromak or an FRC could be formed depending on the helicity ratio of the two initial spheromaks. This was a “relaxation” in that the bifurcation of *preferred states* depended in a repeatable way on the initial conditions. However, a minimization principle by which the “end state” is regulated by certain invariants was not identified. Further, the final poloidal flux was not higher than the initial poloidal flux of either spheromak, and the final state was not quiescent, tending to rapidly develop a tilt instability in the case without using a stabilizing central conducting column [6].

Recent experiments at the Translation, Confinement, and Sustainment (TCS) facility [7] introduced a more complete set of diagnostics, especially highly time- and

space-resolved internal magnetic field profiles, and rotational flow profiles. These measurements have demonstrated, for the first time, that the transition from an early highly dynamical state to the final equilibrium approximately preserves the magnetic helicity, while converting toroidal to poloidal flux. Moreover, the final state is quiescent with high β ; i.e., it is clearly not a Taylor state. This strongly suggests that a more general principle regulates the relaxation. This Letter presents these results.

A sketch of TCS, with the LSX/mod θ -pinch (originally used for FRC acceleration experiments [8]) attached, is shown in Fig. 1. Plasmoids formed in LSX/mod had typical conditions of external axial field $B_e = 0.3$ T, electron density $n_e = 6 \times 10^{20} \text{ m}^{-3}$, and total temperature $T_e + T_i = 400$ eV. The plasmoids were ejected from the LSX/mod *source*, and translated, at ~ 300 km/s, about 4 times the Alfvén speed, into the large-diameter TCS *confinement* section, where a lower bias field (~ 0.05 T) was imposed by external, flux-conserving coils. It then rebounded several times from end mirrors before settling into a quiescent equilibrium, as shown by the space-time history of diamagnetism in Fig. 2. The final confined FRC-like object had a separatrix radius $r_s \sim 0.22$ m, $n_e = 4 \times 10^{19} \text{ m}^{-3}$, $T_e + T_i = 200$ eV.

It is evident from Fig. 2 that the excluded flux $\Delta\phi$ increases substantially between first and second passes through TCS (from 7 to 15 mWb). Also the flux lifetime during the equilibrium phase is even longer than given by the previous R^2/ρ_i scaling measured in nontranslated,

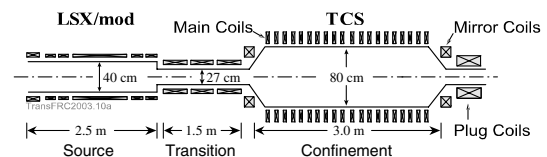


FIG. 1. Schematic of TCS with LSX/mod attached.

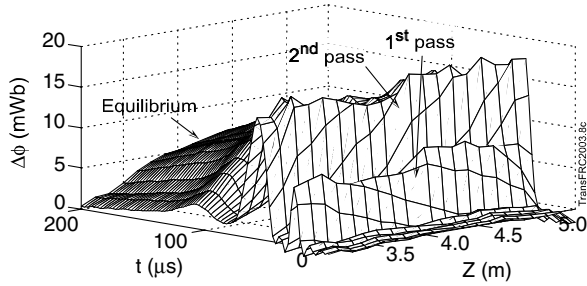


FIG. 2. Evolution of diamagnetism, $\Delta\phi$, in TCS obtained from a series of 18 external diamagnetic loops. Time is measured from the instant of field reversal in LSX/mod, and distance z is from the center of LSX/mod.

high density, θ -pinch formed FRCs [9]. R is the radius of the field null [$B_z(R) = 0$] and ρ_i is the ion Larmor radius in the external field.

Time histories at the center of TCS of the excluded flux radius $r_{\Delta\phi} = (\Delta\phi/\pi B_e)^{1/2}$, the poloidal flux, and the peak density n_{em} are shown in Fig. 3. Of particular interest is the poloidal flux, defined as

$$\phi_p = \int_R^{r_s} 2\pi r dr B_z. \quad (1)$$

Since determination of ϕ_p requires internal field measurements, it has been common to infer it from the routinely measured $r_{\Delta\phi}$ by assuming a rigid-rotor (RR) profile. The poloidal flux inferred in this way is

$$\phi_p^{RR} = 0.3(r_{\Delta\phi}/r_c)\Delta\phi, \quad (2)$$

where r_c is the flux conserver radius, as shown in Fig. 3 as a solid line. A notable feature of the ϕ_p^{RR} trace is the rise between the first pass and equilibrium. With optimal end-mirror conditions this feature was very repeatable. This rise is similar to observations in the FIX device where the rise appeared when the “plug” mirror ratio was not too

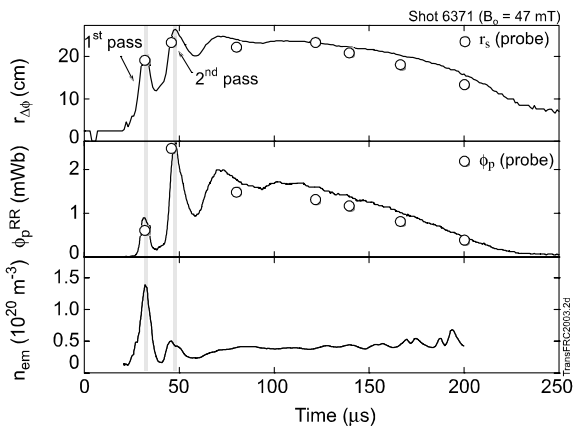


FIG. 3. Properties of a translated FRC. Data points for the separatrix radius, r_s , and the poloidal flux, ϕ_p , are determined from an internal probe. The peak density, n_{em} , is related to the average density from CO₂ interferometry by dividing by $\langle\beta\rangle$.

large [10]. However, the use of ϕ_p^{RR} is of questionable reliability, especially during the dynamic first pass. Thus, internal $B_z(r)$ measurements are essential for determining poloidal flux behavior. The internal field measurements were made at the midplane of TCS using a highly time-resolved magnetic pickup probe with 31 small loops arrayed inside a slender (5 mm diameter) boron nitride covered “sting,” inserted radially downward, up to 12 cm past the axis. ϕ_p , as well as r_s , obtained from the internal probe, is shown in Fig. 3 as a series of discrete points at times when the FRC was centered right and left over the probe, as seen by a 56-chord tomographic system. The internal probe measurements verify, for the first time, that a poloidal flux amplification indeed occurs between the first pass and equilibrium. The separatrix radius r_s inferred from the internal probe is slightly smaller than $r_{\Delta\phi}$ because of the plasma on open field lines.

The jump in poloidal flux has major implications. In an axisymmetric plasma ϕ_p decays at a rate that depends on the resistivity. *It can never increase.* The only way to “amplify” ϕ_p is by a topology-breaking, three-dimensional process that converts toroidal flux into poloidal. *Flux conversion* is a marker of a turbulent relaxation. Flux conversion from toroidal to poloidal is evident from the radial profiles shown in Fig. 4 for the first pass at $\sim 30 \mu s$ and equilibrium at $\sim 140 \mu s$. Several repeatable shots were taken with the internal probe oriented to record either $B_z(y)$ or $B_x(y)$, which represent $B_z(r)$ and $B_\theta(r)$ in a centered axisymmetric plasmoid. (Probe insertion past the axis has clearly shown that the profiles are axisymmetric about the $r = 0$ point shown in Fig. 4.) During the first pass the plasmoid was centered on the internal probe, allowing a front-to-back data sweep. The B_θ reversed from front to back. This differs from the FRX-C/T experiment in which B_θ was unidirectional [11], but agrees with numerical calculations of FRC formation in θ pinches that demonstrated the generation of

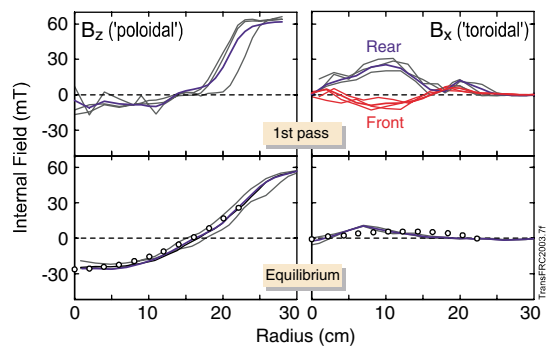


FIG. 4 (color online). Radial profiles of axial and toroidal fields for first pass and equilibrium FRC. The thick solid lines represent the averaged profiles for many shots and time slices. Several individual profiles are also shown to illustrate possible variability. The circles shown during the equilibrium phase are for a Hill’s vortexlike interpretive model.

axially antisymmetric toroidal fields due to poloidally sheared toroidal electron flow [12]. The higher toroidal field in the rear may be caused by the translation process, as in a conical θ pinch [13], which can be reproduced in simulations by including the Hall term [14]. The exact details are not relevant here. More interesting is the transformation (after extremely violent reflections off the end mirrors) from a disorganized plasmoid with low poloidal flux and significant toroidal field to an FRC with enhanced poloidal flux and reduced toroidal flux, defined as $\phi_T = \iint B_\theta dr dz$. Note that in the final equilibrium B_θ is measured only at the midplane, but only the single direction profile shown in Fig. 4 is seen after the first and second reflections, with the peak B_θ monotonically decreasing from the FRC centered value.

Substantial toroidal flow was observed during the equilibrium phase using newly developed multichord Doppler spectroscopy, which monitors the Doppler shift of various impurity lines close to the midplane. The data for C^{++} ions are shown in Fig. 5 during the equilibrium phase. All impurity species, carbon, oxygen, and silicon, exhibited the same rotation rate. Thus, the C^{++} results are assumed to be the same as the bulk deuterium ion rotation. The flow is in the usual ion diamagnetic drift direction. We surmise that plasma flow and angular momentum are extremely important to the displayed FRC robustness, since even the most advanced kinetic calculations of FRC tilt stability without flow do not show such robust stabilization.

An interpretive model is useful to extract global parameters from TCS measurements. For this we introduce a flexible spatial structure for both flows and fields. The structure parameters are adjusted to fit measured quantities. A Hill's vortexlike structure is adopted, with

$$\psi = -\frac{1}{2}B_{z0}r^2\left(1 - \frac{r^2}{a^2} - \frac{z^2}{b^2}\right) \quad (3)$$

(using cylindrical coordinates r, θ, z). The poloidal fields arising from the magnetic flux function inside the separatrix are $B_z = \partial\psi/r\partial r$, $B_r = -\partial\psi/r\partial z$. The toroidal field is specified as

$$B_\theta = B_{\theta0}\frac{r}{a}\left(1 - \frac{r^2}{a^2} - \frac{z^2}{b^2}\right). \quad (4)$$

In the event of a toroidal field structure with changing

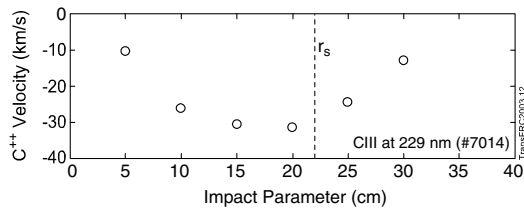


FIG. 5. Flow velocities of C^{++} impurity measured by Doppler spectroscopy during the equilibrium phase (at $\sim 140 \mu s$).

directions, as occurs in the first pass, Eq. (4) is modified by replacing $B_{\theta0} \rightarrow B_{\theta0} + B_{\theta1}z/b$. Note that $B_{\theta1}$ does not contribute to the toroidal flux.

There are four parameters in the model magnetic structure, $a, b, B_{z0}, B_{\theta0}$, except for the first pass where a fifth, $B_{\theta1}$, is added. In the equilibrium phase the four parameters are determined using measurements of the excluded flux radius, volume, poloidal flux, and sectional toroidal flux $\phi'_T \equiv \int_0^{\Delta\phi} B_\theta dr$. The magnetic measurements (as well as interferometric density measurements) are at the midplane of the confinement chamber ($z = 4.25$ m). Equilibrium phase measurements are at $\sim 140 \mu s$. In the first pass, the toroidal flux is inferred as the plasmoid sweeps past the magnetic probes as $\phi_T = u_{tr} \int dt \times \int B_\theta(r, t) dr$, where u_{tr} is the translational velocity of the plasmoid. Thus, there are four measurements to determine the four principal quantities (recall that $B_{\theta1}$ does not contribute to ϕ_T). With these quantities in hand the important global quantities follow. These are poloidal ϕ_p and toroidal ϕ_T fluxes, as well as the magnetic helicity

$$K_m = (2\mu_0 e^2)^{-1} \int d\tau \mathbf{A} \cdot \mathbf{B}, \quad (5)$$

where the integral is over the separatrix volume.

Table I shows the magnetic properties of the plasmoid during the first pass and equilibrium phases. The measured and inferred quantities are listed separately. The last row in Table I shows the change in global quantities from the first pass to equilibrium. Significant flux conversion occurs: a 53% rise in ϕ_p and a 51% drop in ϕ_T . Meanwhile, K_m drops by 26%. This loss is nominally commensurate with the resistive decay time of the flux after the first mirror reflection, but also may be related to the $\sim 50\%$ reduction (as will be seen shortly) in inventory, i.e., the number of ions inside the separatrix. Thus, the magnetic helicity is roughly preserved from the first pass to equilibrium. The circles in Fig. 4 show the fitted structure for the equilibrium phase. Fits are not shown for the first pass since the plasmoid is then highly dynamic. The traces in Fig. 4 are only as smooth as shown due to taking $2 \mu s$ averages for all probe signals. The fitted structure for ϕ_p corresponds to an average of experimental data precisely through the O point. This is also the value plotted in Fig. 3.

TABLE I. Magnetic properties (FP: first pass; EQ: equilibrium).

| | Measured | | Inferred | | | |
|--------|------------|------------------|-------------------|----------------------|-------------------|---------------|
| | a (m) | V (m^3) | ϕ_p (mWb) | ϕ'_T (mWb/m) | ϕ_T (mWb) | K_m (Jm) |
| FP | 0.19 | 0.19 | 0.65 | | 1.71 | -0.43 |
| EQ | 0.22 | 0.2 | 0.95 | 0.79 | 0.83 | -0.32 |
| Change | | | +53% | | -51% | -26% |

TABLE II. Flow properties (FP: first pass; EQ: equilibrium).

| | Measured | | | Inferred | |
|----|--------------------------------------------|----------------------------|--------------------|-----------------------------|-----------------|
| | n ($\times 10^{20} \text{ m}^{-3}$) | \bar{u}_θ (km/s) | u_{tr} (km/s) | N ($\times 10^{19}$) | W_{mf} (J) |
| FP | 0.89 | | 280 | 1.69 | 3400 |
| EQ | 0.41 | -20.8 | | 0.82 | 13.2 |

Less can be inferred about the flow properties since only the translational velocity and the rotational flow structure during the equilibrium phase have been measured. Nevertheless, it is interesting to make estimates of ion helicity (an ideal two-fluid invariant) by ignoring poloidal flow contributions. The ion helicity is

$$K_i = (2\mu_0 e^2)^{-1} \int d\tau \mathbf{P}_i \cdot \nabla \times \mathbf{P}_i, \quad (6)$$

where $\mathbf{P}_i = m_i \mathbf{u}_i + e\mathbf{A}$ is the ion fluid canonical momentum, and m_i , \mathbf{u}_i are the ion mass and ion fluid velocity. We specify the toroidal flow as having the same form as Eq. (4), with the replacement $B_\theta \rightarrow u_\theta$ and with the addition of a rigid toroidal rotation $\Omega r \hat{\theta}$. The model parameters during the equilibrium phase are inferred from the Doppler flow measurements (Fig. 5). With the density assumed uniform inside the separatrix, the inferred K_i is listed in Table II, along with other measured and inferred parameters. The magnetofluid energy is

$$W_{mf} = \int d\tau (m_i n u_i^2 / 2 + B^2 / 2\mu_0). \quad (7)$$

Both K_i and W_{mf} play prominent roles in two-fluid relaxation principles [2–4].

The ion helicity is estimated as follows. We ignore poloidal flow since we have no poloidal flow measurements, and infer the first-pass toroidal flow in two ways: (1) assume conserved angular momentum between the first pass and equilibrium; (2) assume rotation at the diamagnetic drift speed in the first pass. The former gives $K_i = -0.37 \text{ Jm}$ in the first pass; the latter gives nearly the same, -0.38 Jm . This indicates a 30% loss from the first pass to equilibrium, similar to that for K_m . Contributions of poloidal flow to the first-pass ion helicity are low due to the large value of B_θ . During equilibrium the contribution may be large, e.g., an equilibrium poloidal Mach number of -0.1 (a *negative* sign is suggested by results for minimum-energy states) reduces the loss of K_i to 20%. The *dramatic* loss in magnetofluid energy (due to conversion of translational energy to thermal energy) is also consistent with the conjecture of the modern relaxation principle [2,3].

One final observation is that a significant fraction of the inventory ($N \equiv \int n d\tau$) is lost between the first-pass and

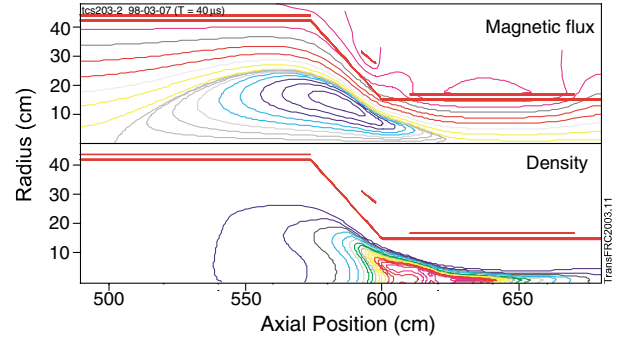


FIG. 6 (color online). Details of MHD calculation of first reflection.

equilibrium states. This is not surprising in view of 2D MHD calculations. Results from the MOQUI code [14] show that in the first reflection the majority of particles concentrate in a small region at the front, extending well into the downstream mirror (Fig. 6). It is expected that the sharp density gradients here produce a large particle loss. The calculated distortions of the flux are much less severe so that flux related quantities may not be so severely affected. It is noteworthy that stable high- β states can result from such a violent process.

The authors thank G. R. Votroubek (tomography), A. M. Peter (velocity flow diagnostic), and the RPPL staff for operating the LSX/mod-TCS facility. Helpful discussions with J. A. Grossnickle, R. D. Milroy, Z. A. Pietrzyk, and J. T. Slough are acknowledged. This work was funded by the U.S. Department of Energy.

-
- [1] J. B. Taylor, Phys. Rev. Lett. **33**, 1139 (1974).
 - [2] L. C. Steinhauer and A. Ishida, Phys. Rev. Lett. **79**, 3423 (1997).
 - [3] L. C. Steinhauer and A. Ishida, Phys. Plasmas **5**, 2609 (1998).
 - [4] Z. Yoshida and S. M. Mahajan, Phys. Rev. Lett. **88**, 095001 (2002).
 - [5] Y. Ono *et al.*, Nucl. Fusion **39**, 2001 (1999).
 - [6] C. D. Cothran *et al.*, Phys. Plasmas **10**, 1748 (2003).
 - [7] A. L. Hoffman *et al.*, Fusion Sci. Technol. **41**, 92 (2002).
 - [8] A. L. Hoffman *et al.*, Fusion Technol. **36**, 109 (1999).
 - [9] A. L. Hoffman and J. T. Slough, Nucl. Fusion **33**, 27 (1993).
 - [10] H. Himura, S. Okada, S. Sugimoto, and S. Goto, Phys. Plasmas **2**, 191 (1995).
 - [11] M. Tuszewski and B. L. Wright, Phys. Rev. Lett. **63**, 2236 (1989).
 - [12] Yu. A. Omelchenko, Phys. Plasmas **7**, 1443 (2000).
 - [13] K. Wira and Z. A. Pietrzyk, Phys. Fluids B **2**, 561 (1990).
 - [14] R. D. Milroy and J. U. Brackbill, Phys. Fluids **29**, 1184 (1986).